Low-lying resonances and relativistic screening in Big Bang Nucleosynthesis

M.A. Famiano[1,3],* A.B. Balantekin[2,3],† and T. Kajino[3,4‡]
[1]*Department of Physics, Western Michigan University, Kalamazoo, Michigan 49008, USA*
[2]*Department of Physics, University of Wisconsin, Madison, WI 53706, USA*
[3]*National Astronomical Observatory of Japan 2-21-1 Osawa, Mitaka, Tokyo, 181-8588, Japan and*
[4]*Department of Astronomy, School of Science, The University of Tokyo, 7-3-1 Hongo, Bunkyo-ku, Tokyo, 113-0033, Japan*

We explore effects of the screening due to the relativistic electron-positron plasma and presence of resonances in the secondary reactions leading to $A = 7$ nuclei during the Big Bang Nucleosynthesis. In particular, we investigate and examine possible low-lying resonances in the ^{7}Be(^{3}He, γ)^{10}C reaction and examine the resultant destruction of ^{7}Be for various resonance locations and strengths. While a resonance in the ^{10}C compound nucleus is thought to have negligible effects we explore the possibility of an enhancement from plasma screening that may adjust the final ^{7}Be abundance. We find the effects of relativistic screening and possible low-lying resonances to be relatively small in the standard Early Universe models.

PACS numbers: 26.35.+c,25.55.-e

arXiv:1603.03137v3 [astro-ph.CO] 26 Mar 2016

INTRODUCTION

Observation of the accelerated expansion of the Universe, measurement of the Cosmic Microwave Background Radiation temperature anisotropies and the observation of the light elements produced during the Big Bang Nucleosynthesis (BBN) epitomize the current status of the precision cosmology. Especially the BBN is an ideal tool not only to test aspects of the Standard Models of cosmology as well as of nuclear and particle physics but also to look for new physics beyond those standard models. (For recent reviews of BBN see Refs. [1–4]). In particular new calculations of the light-element abundances are performed [1] using the recent high-precision 2015 *Planck* measurement of the baryon-to-photon ratio, helium abundance and the effective number of relativistic degrees of freedom, $N_{\rm eff}$ [5], as well as astronomical observations of deuterium [6, 7]. These calculations find that D/H observations are now more precise than the corresponding theoretical predictions, but predictions for $A = 7$ nuclei continue to disagree with observations. A recent update (NACRE II) of the compilation of charged-particle-induced thermonuclear reaction rates for nuclei with mass number $A < 16$ [8] was used in the calculations of Refs. [1] and [2]. These calculations also provide confidence limits for the production of ^{6}Li, ^{9}Be, ^{11}B, and carbon, oxygen, and nitrogen (CNO). A precise value of the CNO/H is not only important for population III star formation, but as we elaborate in this paper, may also affect the abundances of $A = 7$ nuclei.

The purpose of the present paper is twofold. One is to explore the plasma effects in the BBN more completely. It was already demonstrated that non-relativistic screening of the Coulomb interaction in nuclear reactions taking place during the BBN epoch does not produce a noticeable impact on light element abundances [9]. However, the screening effects due to the relativistic electron-positron plasma was not included in the analysis of Ref. [9]. It was recently shown that electron-positron plasma screening is crucial for neutrino interactions in the BBN epoch [10]. In the current work we include the effects of the screening due to the electron-positron plasma in nuclear reactions during the BBN epoch. A second purpose is to explore the ramifications of the possible presence of resonances in relatively unexplored reactions involving $A = 7$ nuclei.

EFFECTS FROM SCREENING IN A RELATIVISTIC ELECTRON PLASMA

For a low-density plasma at T$\sim$1 to 2 MeV, non-relativistic screening can be neglected as the associated Debye length is $\lambda_D \sim 10^4$ fm (see Appendix) [9]. For example, for $Z_1 = Z_2 = 2$, and temperature of 1 MeV, one gets $\lambda_D = 10^4$ fm and the Salpeter correction to the reaction rate $f_D - 1 \approx 6\times10^{-4}$. However, for an electron-positron plasma, as would exist in the BBN epoch, the temperature is of the same order as the electron mass, requiring the relativistic expression (given in the Eq. (A.17) of Appendix). For a vanishing chemical potential, this Debye length as a function of temperature is shown in Figure 1. At higher temperatures, this is much smaller than the Debye length which was determined for screening by non-relativistic electrons alone.

Using this Debye length, we used a BBN nuclear reaction network to determine the change in mass fractions based on the screening enhancement factor. Corrections were made to reaction rates in the network by inserting the Debye length for a relativistic plasma into Eq. (A.19). The reaction network used is shown in Figure 2. Reactions up to and including $Z = 6$ were included, as well as weak rates and decays.

Mass fractions $X_{\rm bare}$ were determined using a network

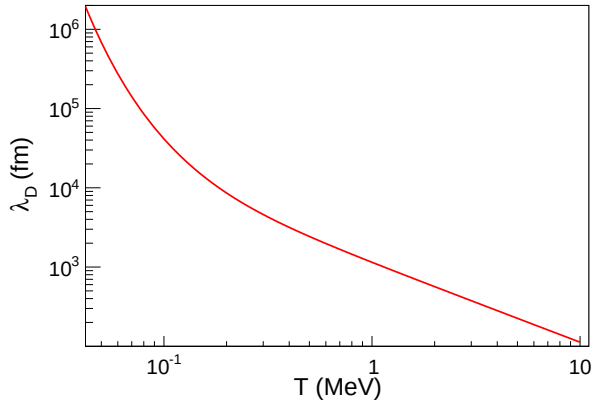

FIG. 1: The Debye length for a relativistic electron plasma as a function of temperature at $\mu = 0$.

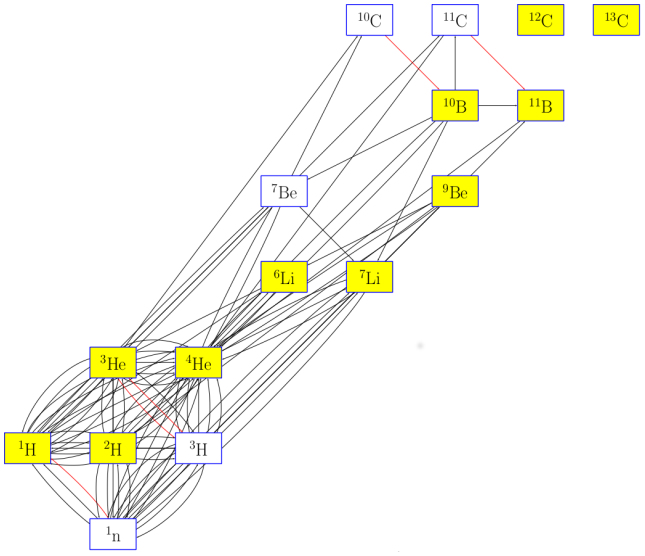

FIG. 2: The BBN reaction network used up to and including nuclei $Z = 6$.

with unscreened rates. These are compared to mass fractions $X_{\rm scr}$ from a network employing rates from reactions screened by a relativistic electron plasma. The change in mass fraction:

$$\frac{\Delta X}{X} \equiv \frac{X_{\rm scr} - X_{\rm bare}}{X_{\rm bare}} \qquad (1)$$

is shown in Figure 3. At early times in the network, the temperature is higher, and the consumption of protons, deuterium, and helium proceeds at a higher rate for the screened reactions compared to the unscreened case. The overall net destruction of these lighter elements is higher in the screened case. While there is an overall reduction in some of the heavier elements, the relative change for those is extremely small. Reaction screening is likely to be small in the regime of zero electron chemical potential.

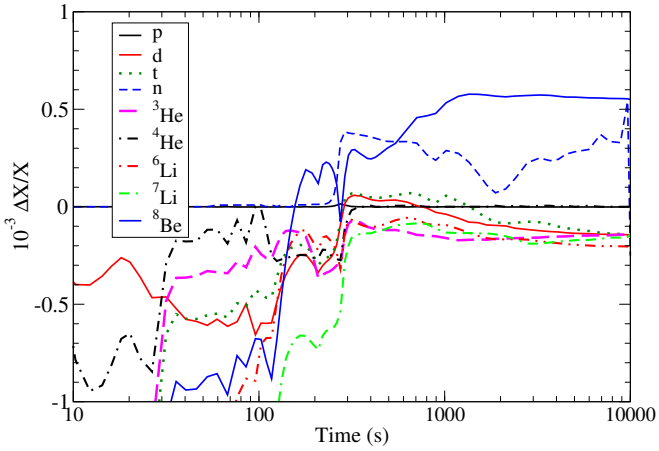

FIG. 3: Relative change in mass fractions for nuclei in the BBN network as a function of time.

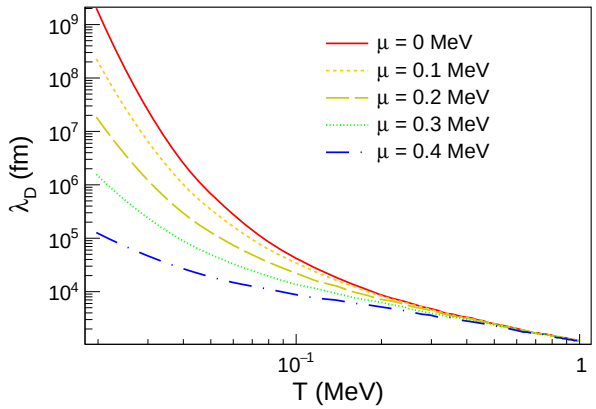

FIG. 4: Debye length as a function of temperature in an electron plasma for non-zero chemical potential for various chemical potentials.

Non-Zero Chemical Potential

Inclusion of a non-zero chemical potential in Equation A.17 will increase the inverse screening length and thus decrease the Debye length, thus increasing the reaction rate enhancement factor.

For a non-zero chemical potential, Equation A.17 was solved numerically. The Debye length, λ_D, for various chemical potentials, μ, as a function of temperature is shown in Figure 4. A somewhat large chemical potential is necessary for a reduction in the Debye length by one order of magnitude, and this occurs only at low temperature. At higher temperatures, the electron kinetic energy dominates over the chemical potential, and the effect of μ is reduced. The resulting enhancement factor, f_D, is shown in Figure 5 for $Z_1 = Z_2 = 2$. From this figure, one sees that for zero chemical potential the enhancement factor changes more rapidly at low temperature than at

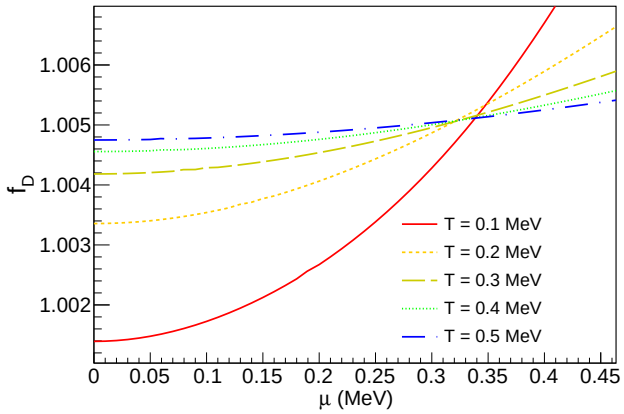

FIG. 5: Reaction rate enhancement factor as a function of the electron chemical potential for temperatures $T = 0.1$ through 0.5 MeV with $Z_1 = Z_2 = 2$.

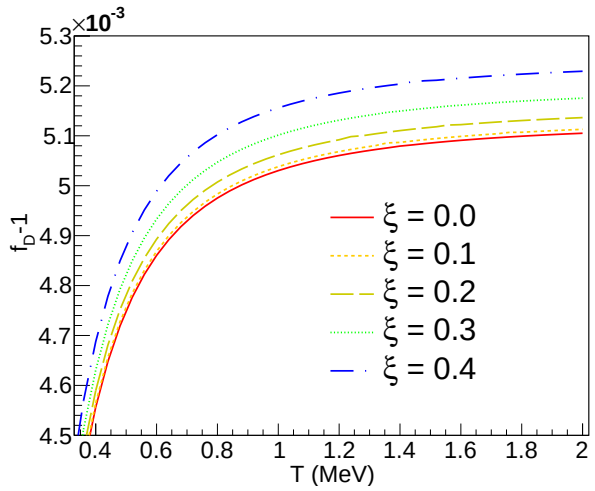

FIG. 6: The reaction rate enhancement factor as a function of temperature for various electron degeneracy factors with $Z_1 = Z_2 = 2$. In this figure, $f = f_D(\mu \neq 0)$.

high temperature. As the temperature approaches the value of the electron mass, the enhancement factor increases less rapidly. One also sees that the enhancement factor as a function of μ changes much less at higher temperatures than at lower temperatures.

It is customary to relate the chemical potential to the electron degeneracy parameter:

$$\xi = \frac{\mu}{T}. \tag{2}$$

Assuming a constant degeneracy parameter, then the chemical potential is much lower at lower T, reducing the effect of μ at lower T. This is shown in Figure 6. One sees that, because the chemical potential now is a linear function of temperature, there is little change in the enhancement factor with degeneracy.

It is thus concluded that, since the electron degeneracy is very small, screening from the relativistic electron-positron plasma has little effect on the final abundance distribution in the standard BBN.

REDUCTION OF ^{7}BE FROM REACTIONS ON ^{3}HE

There is significant discrepancy between the observations and the BBN predictions for $A = 7$ nuclei, known as the "lithium problem". (For an overview of the current status of the lithium problem see Ref. [11]). One alternative mechanism for the possible reduction of ^{7}Li was proposed in Ref. [12], namely that the consumption of ^{7}Be (and subsequently ^{7}Li) may occur through a resonant reaction through the ^{10}C compound nucleus:

$$^7\mathrm{Be} + ^3\mathrm{He} \rightarrow ^{10}\mathrm{C}^* \quad \rightarrow ^{10}\mathrm{C} + \gamma \tag{3}$$

$$\rightarrow ^9\mathrm{B} + p \tag{4}$$

$$\rightarrow 2\alpha + 2p \tag{5}$$

While this reaction has certainly been previously explored [13], here it is investigated in light of possible resonance structure in the mirror product ^{10}Be [14], particularly at resonant energies greater than 0.5 MeV. Prior studies have not found resonances in the ^{10}C nucleus [13] for relatively large widths in the range $E_R < 500$ keV. This work examines resonances both within and outside the energy range and widths previously investigated where the effects of a relativistic electron-positron plasma on BBN reaction rates are included. We examine the possible effects of shifts in the thermonuclear reacstion rates for resonant and non-resonant reactions from a relativistic electron plasma.

Resonances in ^{7}Be+^{3}He

Taking the resonance structure of ^{10}Be as motivation, a resonance is assumed for the ^{7}Be+^{3}He reaction. We note that this reaction and any possible resonances within this reaction have been shown to have a negligible effect on BBN [15]. Likewise, there is no experimental evidence for resonances below 500 keV [13]. The effects of screening in the hot BBN plasma from electrons and positrons has been investigated neither on the non-resonant nor resonant rates. Any possible resonances at $E_R > 500$ keV and their corresponding strengths are not known. The decay width Γ of the ^{10}Be mirror nucleus for the 17.79 MeV state (0.53 MeV above the reaction threshold) is known to be 110 ± 35 keV [16] though the entrance channel width has not been experimentally determined.

We assume a resonance cross section of the form

$$\sigma(E) = \pi\lambda^2\omega\gamma\frac{\Gamma_{\mathrm{total}}}{(E - E_R)^2 + \Gamma^2_{\mathrm{total}}/4} \tag{6}$$

where

$$\Gamma_{\rm total} = \Gamma_{\rm in} + \Gamma_{\rm out}, \tag{7}$$

γ is the reduced width

$$\gamma = \frac{\Gamma_{\rm in}\Gamma_{\rm out}}{\Gamma_{\rm total}}, \tag{8}$$

λ is the de Broglie wavelength, and ω is the appropriate spin factor.

In the current study, final BBN mass fractions are determined for reaction rates based on a single resonance E_R of arbitrary strength $\omega\gamma$. The mass fractions are determined as a function of these two parameters.

The partial width for the entrance channel is derived from a solution to the spherical wave equation at the nuclear potential radius, and the functional form is [17]:

$$\Gamma_p(E) = 2P_L(E)\gamma_L(a)^2 \tag{9}$$

where the factor γ_L is the reduced particle width at a radius a and is given in the Wigner limit as:

$$\gamma_L^2(a) = \theta_L^2(a)\gamma_W^2(a) = \theta_L^2\frac{3\hbar^2}{2m_{12}a^2} \tag{10}$$

and the penetrability factor P_L is given by the regular (F_L) and irregular (G_L) Coulomb functions:

$$P_L(a) = \frac{ka}{F_L^2(ka)+G_L^2(ka)} = \frac{\rho}{F_L^2(\eta,\rho)+G_L^2(\eta,\rho)} \tag{11}$$

where η is the Sommerfeld parameter and $\rho \equiv ka$. These are evaluated numerically at the nuclear radius. In this case, only the $L = 0$ terms are used, and the single-particle width $\theta_L^2 = 0.5$ is assumed.

The entrance channel width at lower energies is shown in Figure 7 for the ^{7}Be+^{3}He reaction. Near threshold, the particle width drops precipitously, while above threshold, it increases to a substantial value. The effect of the energy-dependent width can be shown in Figure 8 which shows the integrand of the thermonuclear rate at $T = 1$ MeV for a resonance $E_R = 500$ keV. The high energy tail of the resonance can have a large effect on the overall rates.

Relativistic electron-positron screening can adjust the incident particle energy, effectively shifting the threshold energy in the cross-section. One can see that for near-threshold or sub-threshold resonances, this shift could result in a significant chance in the cross-section, as discussed in the next section.

In addition to the above resonance structure, we determined BBN abundance distributions for a range of narrow resonances and strengths. By scanning across strengths and resonance locations, the relative reduction of ^{7}Be was mapped. The mapping of the relative mass

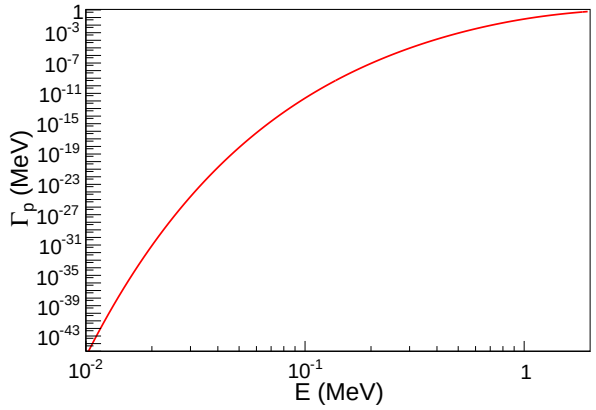

FIG. 7: The assumed entrance channel width as a function of incident particle energy for the ^{7}Be(^{3}He,γ)^{10}C reaction.

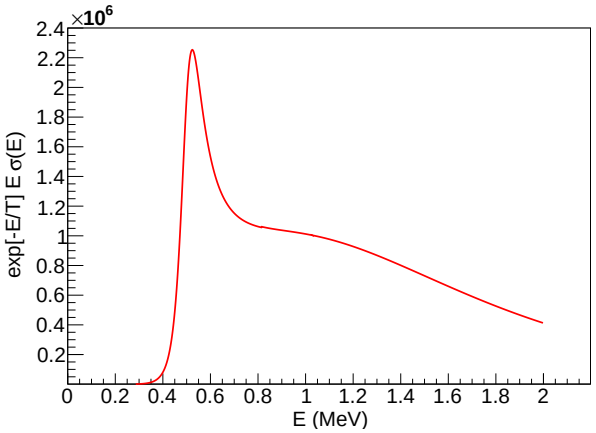

FIG. 8: The integrand of the thermonuclear reaction rate for the energy-dependent width of the ^{7}Be(^{3}He,γ)^{10}C reaction at T=1 MeV for a resonance located at E_R=500 keV.

fraction of ^{7}Be, R, is defined to be the final ^{7}Be mass fraction for a BBN calculation with a ^{10}C resonance divided by that with no resonance:

$$R \equiv \frac{X_{res}}{X_{nr}} \tag{12}$$

RELATIVISTIC ELECTRON SCREENING AND THE ^{7}BE+^{3}HE REACTION

Prior to examining resonances in the ^{7}Be+^{3}He reaction, we proceed with a discussion of the effects of relativistic electron screening on the same reaction.

While a resonance in ^{10}C may increase the destruction of ^{7}Be, the effect may be magnified by the inclusion of screening from the electron plasma. The enhancement on the cross section is described in the Appendix. Incorporating screening into the usual thermonuclear reaction

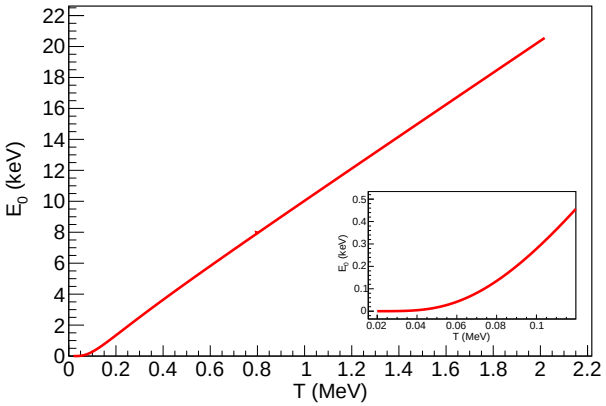

FIG. 9: The energy shift E_0 due to relativistic screening as a function of temperature for Z_1=2, Z_2=4, and μ=0. The high temperature limit is as given in Equation A.23. The inset shows the shifts at low temperature.

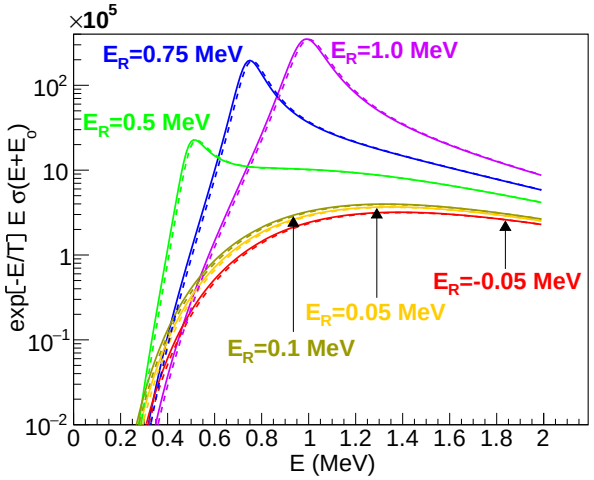

FIG. 10: The integrand of the reaction rate for a narrow resonance for three values of the resonance energies for the bare potential (dotted lines) and the screened potential (solid lines). For the low-lying resonances, the resonance at 0.1 MeV corresponds to the upper-most set of lines, while the resonance at -0.05 MeV corresponds to the lowest set of lines.

rate (TRR) will create an energy shift E_0 of the reaction system because of the reduced particle potential. The energy shift E_0 is defined in the appendix.

This shift is small, $\sim$ 20 keV for $Z_1 = 2$ and $Z_2 = 4$ at $T \sim 2$ MeV. The values of ΔE as a function of temperature are shown in Figure 9; the trend is nearly linear except at low temperature. Its effect on non-resonant TRRs is also expected to be small, particularly as the cross-section is negligible near $E = 0$. However, the shift could be significant for resonant rates, particularly those low-lying resonances near the threshold, where even a small shift in the energy can result in a significant change in the cross-section.

Another possible effect of this shift is the influence on sub-threshold resonances. A shift to higher energy can result in a much more significant decrease in the cross-section and total reaction rate as less of the sub-threshold resonance is integrated over. Using this shift, a possible reduction in the TRR for low-lying resonances is investigated. The result may be significant because the energy shift results in less of the resonance tail being included in the TRR. From Figure 9, one expects the enhancement to be small, approximately 1%, and to scale with temperature. This scaling is because as the temperature decreases the Debye screening length increases, resulting in a reduced energy shift, which approaches zero. This is important to note as the effect is most pronounced only at high temperatures (early in BBN) and in regions where a significant portion of the resonance may be removed from the reaction rate - near the threshold. This may be advantageous as there may be a slight reduction in BBN reaction rates during the early stages, resulting in a slower progression to the $A = 7$ nuclei.

The effect of this shift is shown in Figure 10 which shows a resonance ($\Gamma_x = 110$ keV, $T = 1$ MeV) in the ^{7}Be $+^3$He reaction times the Boltzmann distribution for six values of E_R. This quantity is the integrand of equation A.26. For this quantity, the particle energy is dictated by the Boltzmann distribution while the value of the cross section is determined by the energy shift (to higher energy), effectively shifting the cross-section to lower energy in the particle distribution. We note, of course, that the lowest resonances in this figure have been eliminated by experiment, but they are shown here to indicate the relative strengths of the resonance tails and to emphasize the point that the actual resonance peaks are not important as the penetrability in the entrance channel at the lowest energies reduces the cross-section to negligible values.

For all resonances shown, the shift to higher energy shifts the entire integrand towards the high-energy tail of the resonance. For the low-lying resonances, $E_R \lesssim 500$ keV, the integral is increased slightly as the tail of the integrand is emphasized. For a higher-energy resonance, $E_R \gtrsim 500$ keV, only a very small portion of the lower energy tail is cut out of the integration, as most of the low-energy tail is dominated by the entrance channel penetrability.

The enhancement for non-resonant rates is exemplified in Figure 11 for $Z_1 = 2$ and $Z_2 = 4$. As expected, the enhancement is small and always greater than unity at non-zero temperature since the cross-section is always monotonically increasing with energy and a small shift to positive energy results in a larger cross section integrated into the reaction rate. It was found that this enhancement varies little with resonance energy and width. This makes sense considering the integrand of the reaction rate and the very small energy shift ΔE. In any case, essen-

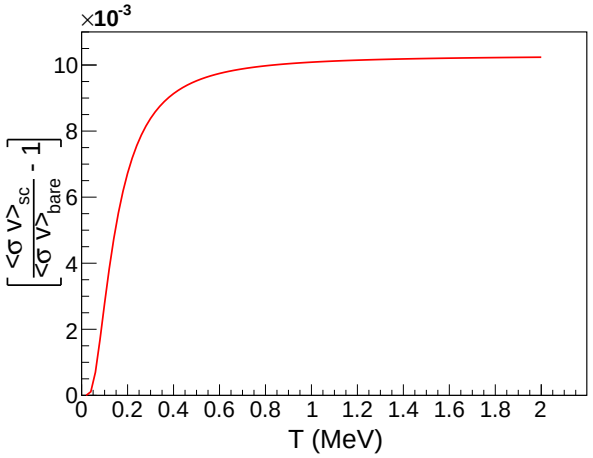

FIG. 11: Ratio of screened to bare TRR for the non-resonant component of the TRR only.

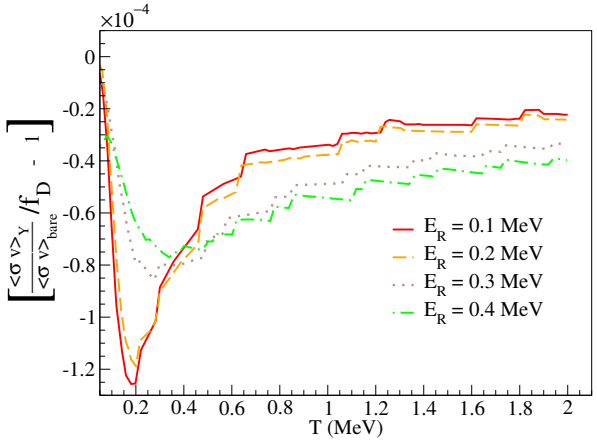

FIG. 12: The correction to the reaction rate from the energy shifts as studied in this work divided by the Salpeter correction factor for several resonance energies, indicated in the figure.

tially the entire cross-section is integrated over, but it is effectively shifted to a higher energy in the Maxwell-Bolzmann distribution by an amount ΔE. For a very small shift, the ratio of rates in Figure 11 is roughly:

$$\frac{R_{sc}}{R_{bare}} \sim e^{\Delta E/T} \tag{13}$$

which is the Salpeter factor.

Accuracy of the Salpeter Approximation

In the previous section, the exact integration of Equation A.26 was used to determine the correction to reaction rates for the relativistic electron gas. The typical prescription is to use the Salpeter approximation to determine the width corrections. This approximation results from the separation of the exponent containing the Debye length from the integration over energy and use as an independent coefficient in the reaction rate without shifting the cross section energy.

This correction can be evaluated by considering the change in reaction rates using the exact screening due to the Coulomb potential in the Yukawa form compared with the Salpeter approximation. This evaluation is shown in Figure 12 where we plot the quantity

$$\left(\frac{<\sigma v>_{\rm Yukawa}}{<\sigma v>_{\rm bare}}\right) \Big/ f_D. \tag{14}$$

In Figure 12, we take $\Gamma_\gamma = 110$ keV, $\Gamma_p = 2$ keV corresponding to $E_R \approx 500$ keV, and the difference between the ratio in Equation (14) and unity is multiplied by 10^4. It can be seen that the relative difference between the correction in Figure 12 and the Salpeter correction factor is on the order of 10^{-4}. The small energy shifts from electron screening induce a difference ratio nearly equal to the Salpeter correction factor to within $\approx 0.01\%$, though it does appear that the difference gets larger at lower temperatures and lower resonance energies as more of the resonance falls below the reaction threshold for the energy shifts induced by screening.

Thermonuclear Reaction Rates (TRRs) for Various Resonances

TRRs for this reaction are shown in Figure 13 for several resonances. For these resonances, we assume a total ^{10}C decay width $\Gamma_x = 110$ keV, a spin degeneracy factor $\omega = 0.5$, and a single particle width $\theta_L^2 = 0.5$. The thermonuclear rates are shown only for the resonances and must be added to the non-resonant rate, also shown in the figure. We observe that the results in Figure 13 decrease with the decay width. For decay widths $\Gamma_x \lesssim 50$ keV, the resonant rates are less than the non-resonant rate.

It is seen that the rates are similar for all the resonances in this temperature range. Several factors must be considered. First, for the energy-dependent widths, a lower resonance may have a larger particle population in the Maxwell-Boltzmann distribution, but the entrance channel widths are also smaller. Very roughly, the rate is proportional to the penetrability factor times the Maxwell-Boltzmann factor. While the penetrability factor increases with energy, the Maxwell-Boltzmann factor decreases.

From the Figure 13 one can conclude that resonances in the energy range of 0≤E≤1 MeV and with $\Gamma_x < 110$ keV for the ^{7}Be+^{3}He reaction are insufficient for reducing the BBN production of ^{7}Be. This is consistent with prior results [15], and the additional inclusion of relativistic plasma screening effects have also been found to be

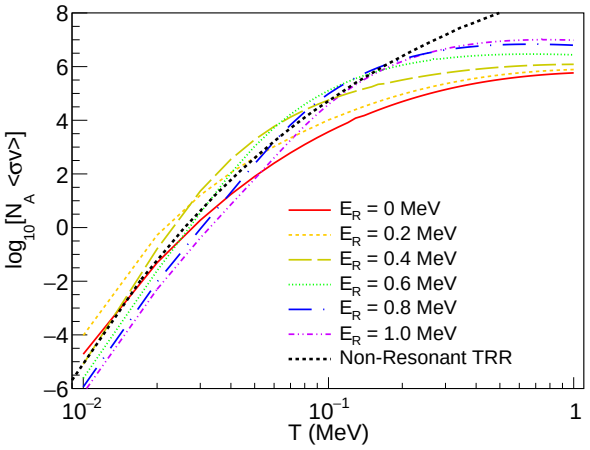

FIG. 13: Thermonuclear reaction rates for the ^{7}Be(^{3}He,γ)^{10}C reaction for several resonances for possible particle-decay channels in the ^{10}C compound nucleus. The dashed black line is the non-resonant TRR. Assumptions are described in the text.

negligible. Thus, the validity of the previous analysis is maintained. A possible BBN scenario with a higher density at lower temperatures may result in such a situation, though one must gauge the effects of the density increase on other reactions as well.

CONCLUSIONS

In this work we explored in detail the consequences of the screening due to the relativistic electron-positron plasma on non-resonant and possible resonances on the secondary reactions destroying $A = 7$ nuclei during the Big Bang Nucleosynthesis. We found that effects of screening from the relativistic plasma are small even for the reaction with the largest Z_1Z_2, namely ^{3}He+^{7}Be. We note that this reaction remains to be the least experimentally explored one in the network of BBN reactions.

We scanned through possible resonance parameters (widths and resonance energies) in our calculations. The very small entrance channel widths in any possible resonance renders its effects quite small. BBN reactions would have to overcome this either by resonances to high spin states - which is very unlikely, resonances via neutron captures to destroy A=7 nuclei - which are inhibited by an insufficient neutron abundance by the time A=7 nuclei are produced, or via resonances to energy states high above threshold. As the temperature by the time A=7 nuclei are produced in significant abundance is low ($T_9 \sim 1$), this last case is also not highly probable.

Even though the effects we find are small, it still is worthwhile to demonstrate how robust our current understanding of the BBN is to effects not previously considered. This is especially important since the instruments scheduled to go online in the future, such as the Thirty Meter Telescope [18], will measure the abundances of the light elements resulting from the BBN with greater precision.

MAF and ABB would like to thank the members of of the National Astronomical Observatory of Japan for their hospitality. This work was supported in part by Grants-in-Aid for Scientific Research of JSPS (26105517, 24340060) of the Ministry of Education, Culture, Sports, Science and Technology of Japan, in part by the US National Science Foundation Grants No. PHY-1204486 at Western Michigan University (WMU) and PHY-1514695 at the University of Wisconsin, in part by a WMU Support for Faculty Scholars Award and in part by the University of Wisconsin Research Committee with funds granted by the Wisconsin Alumni Research Foundation.

Appendix: Screening of the Coulomb potential

In a plasma the Coulomb potential between two nuclei is screened:

$$V_C^{\rm scr} = \frac{Z_1 Z_2 e^2}{r} \exp\left(-\frac{r}{\lambda_D}\right) \qquad \text{(A.15)}$$

where λ_D is the Debye radius. The non-relativistic contribution to the Debye radius is given by

$$\lambda_D = \left[\frac{T}{4\pi e^2 N\left(\sum_i X_i \frac{Z_i^2}{A_i} + \xi \sum_i X_i \frac{Z_i}{A_i}\right)}\right]^{1/2} \qquad \text{(A.16)}$$

where N is the ion number density, X_i is the mass fraction of nuclei of type i, and ξ is a factor that accounts for the electron degeneracy [19]. Eq. (A.16) is derived using non-relativistic limit, which is appropriate for the nuclei in the Big Bang. This formula was used in the calculations of Ref. [9].

Contribution to the Debye length from the relativistic electron-positron plasma can be calculated exactly to all orders from the Schwinger-Dyson equation for the photon propagator [20]. It is given as

$$\frac{\pi^2}{\lambda_D^2} = e^2 \frac{\partial}{\partial \mu} \int_0^\infty dp p^2 \left[\frac{1}{e^{(E-\mu)/T}+1} - \frac{1}{e^{(E+\mu)/T}+1}\right], \qquad \text{(A.17)}$$

where $E = \sqrt{p^2 + m_e^2}$ and μ is the chemical potential.

The correction to the reaction rates,

$$\langle \sigma v \rangle = \frac{1}{\pi m_{12}} \left(\frac{2}{T}\right)^{3/2} \int_0^\infty e^{-E/T} E \sigma(E) dE, \qquad \text{(A.18)}$$

due to the plasma effects was first calculated by Salpeter [19]. He found that the rates are enhanced by a factor of

$$f_D = \exp\left(\frac{Z_1 Z_2 e^2}{T \lambda_D}\right). \qquad \text{(A.19)}$$

A comparison of different derivations of the Salpeter's plasma correction is given in Ref. [21]. Here we outline another derivation which illustrates the behavior of enhancement in the presence of resonances. The dynamics of two colliding nuclei in a plasma below the Coulomb barrier is described by [22]

$$H^{\rm scr}\Psi = E\Psi \tag{A.20}$$

where

$$H^{\rm scr} = T + V_N + V_C^{\rm scr}. \tag{A.21}$$

For $r \ll \lambda_D$, the screened Coulomb potential of Eq. (A.15) can be expanded as

$$V_C^{\rm scr} \sim V_C^{\rm bare} - \frac{Z_1 Z_2 e^2}{\lambda_D} = V_C^{\rm bare} - E_0. \tag{A.22}$$

In the high temperature limit, Equation A.17 yields:

$$E_0 = \frac{Z_1 Z_2 e^3}{\pi}\left[\mu^2 + \frac{\pi^2}{3}T^2\right]^{1/2} \tag{A.23}$$

Inserting Eq. (A.22) into Eq. (A.20) one gets

$$H^{\rm bare}\Psi = (E + E_0)\Psi \tag{A.24}$$

where

$$H^{\rm bare} = K + V_N + V_C^{\rm bare} \tag{A.25}$$

with K being the kinetic energy associated with the relative motion of the nuclei and V_N is the attarctive nuclear potential. Hence the effect of the screening is to shift the energy by an amount E_0 in the calculations performed using the bare Coulomb potential. As a result the reaction rate takes the form

$$\langle\sigma v\rangle = \frac{1}{\pi m_{12}}\left(\frac{2}{T}\right)^{3/2}\int_0^\infty e^{-E/kT} E\sigma(E + E_0)dE. \tag{A.26}$$

After a change of variables $E' = E + E_0$, the rate then takes the form

$$\langle\sigma v\rangle \sim \int_{E_0}^\infty e^{-(E'-E_0)/T}(E' - E_0)\sigma(E')dE'. \tag{A.27}$$

Since E_0 is very small the lower limit of the integral can be extended to zero and the term linear in E_0 multiplying the cross section can be ignored. In Ref. [23] it was shown that the correction due to these approximations is indeed very small. The E_0/T contribution to the exponential yields the Salpeter enhancement of Eq. (A.19). Note that Eq. (A.26) demonstrates that a shift away or towards the peak energy can appreciably alter the reaction rates in the presence of resonances.

* Electronic address: michael.famiano@wmich.edu
† Electronic address: baha@physics.wisc.edu
‡ Electronic address: kajino@nao.ac.jp

[1] R. H. Cyburt, B. D. Fields, K. A. Olive and T. H. Yeh, arXiv:1505.01076 [astro-ph.CO].
[2] A. Coc, J. P. Uzan and E. Vangioni, JCAP **10**, 050 (2014).
[3] F. Iocco, G. Mangano, G. Miele, O. Pisanti and P. D. Serpico, Phys. Rept. **472**, 1 (2009).
[4] G. Steigman, Ann. Rev. Nucl. Part. Sci. **57**, 463 (2007).
[5] P. A. R. Ade *et al.* [Planck Collaboration], arXiv:1502.01589 [astro-ph.CO].
[6] S. Burles and D. Tytler, Astrophys. J. **499**, 699 (1998). Astrophys. J. **507**, 732 (1998). D. Kirkman, D. Tytler, N. Suzuki, J. M. O'Meara and D. Lubin, Astrophys. J. Suppl. **149**, 1 (2003).
[7] R. Cooke, M. Pettini, R. A. Jorgenson, M. T. Murphy and C. C. Steidel, Astrophys. J. **781**, no. 1, 31 (2014). M. Pettini and R. Cooke, Mon. Not. Roy. Astron. Soc. **425**, 2477 (2012).
[8] Y. Xu, K. Takahashi, S. Goriely, M. Arnould, M. Ohta and H. Utsunomiya, Nucl. Phys. A **918**, 61 (2013).
[9] B. Wang, C. A. Bertulani and A. B. Balantekin, Phys. Rev. C **83**, 018801 (2011).
[10] N. Vassh, E. Grohs, A. B. Balantekin and G. M. Fuller, Phys. Rev. D **92**, 125020 (2015).
[11] B. D. Fields, Ann. Rev. Nucl. Part. Sci. **61**, 47 (2011).
[12] N. Chakraborty, B. D. Fields and K. A. Olive, Phys. Rev. D **83**, 063006 (2011).
[13] F. Hammache, A. Coc, N. deSereville, I. Stefan, P. Roussel, S. Ancelin, M. Assie, L. Audouin, D. Beaumel, S. Franchoo, B. Fernandez-Dominguez, S. Fox, C. Hamadache, J. Kiener, A. Laird, B. LeCrom, A. Lefebvre-Schuhl, L. Lefebvre, I. Matea, A. Matta, G. Mavilla, J. Mrazek, P. Morfouace, F. deOliveiraSantos, A. Parikh, L. Perrot, A.M. Sanchez-Benitez, D. Suzuki, V. Tatischeff, P. Ujic, and M. Vandebrouck, Phys. Rev. C **88**, 062802 (2013).
[14] J. Yan, F. E. Cecil, U. Greife, C. C. Jewett, R. J. Peterson and R. A. Ristenin, Phys. Rev. C **65**, 048801 (2002).
[15] C. Broggini, L. Canton, G. Fiorentini, and F.L. Villante, JCAP **06**, 30 (2012).
[16] F. Ajzenberg-Selove, Nucl. Phys. A **413**, no. 1, 1 (1984).
[17] C. Iliadis, *Nuclear Physics of Stars*, (Wiley-VCH, Weinheim, 2007).
[18] W. Skidmore *et al.*, arXiv:1505.01195 [astro-ph.IM].
[19] E. E. Salpeter, Austral. J. Phys. **7**, 373 (1954).
[20] J. I. Kapusta and C. Gale, *Finite-temperature field theory: Principles and applications* (Cambridge University Press, Cambridge, 2006).
[21] J. N. Bahcall, L. S. Brown, A. Gruzinov and R. F. Sawyer, Astron. Astrophys. **383**, 291 (2002).
[22] A. B. Balantekin and N. Takigawa, Rev. Mod. Phys. **70**, 77 (1998).
[23] J. N. Bahcall, X. Chen and M. Kamionkowski, Phys. Rev. C **57**, 2756 (1998).